The Version of Record of this manuscript has been published and is available in Canadian Journal of Remote Sensing: http://www.tandfonline.com/10.1080/07038992.2019.1573136

Evaluation of Chinese Quad-polarization Gaofen-3 SAR Wave Mode Data for Significant Wave Height Retrieval

Shuai Zhu[1], Weizeng Shao[1*], Armando Marino[2], Jian Shi[3], Jian Sun[4], Xinzhe Yuan[5], Jiachen Hu [1], Dongkai Yang[6] and Juncheng Zuo[1]

1. Marine Science and Technology College, Zhejiang Ocean University, Zhoushan, China
2. Natural Sciences, University of Stirling, Stirling, UK
3. College of Meteorology and Oceanography, National University of Defense Technology, Nanjing, China
4. Physical Oceanography Laboratory/CIMST, Ocean University of China and Qingdao National Laboratory for Marine Science and Technology, Qingdao, China
5. National Satellite Ocean Application Service, State Oceanic Administration, Beijing, China
6. School of Electronic and Information Engineering, Beihang University, Beijing, China

---

Abstract

Our work describes the accuracy of the Chinese quad-polarization Gaofen-3 (GF-3) synthetic aperture radar (SAR) wave mode data for wave retrieval and provides guidance for operational applications of GF-3 SAR. In this study, we have evaluated the accuracy of SAR-derived significant wave height (SWH) from 10514 GF-3 SAR images with visible wave streak acquired in wave mode by using the existing wave retrieval algorithms, e.g., the theoretical-based algorithm parameterized first-guess spectrum method (PFSM), the empirical algorithm CSAR_WAVE2 for VV-polarization, and the algorithm for quad-polarization (Q-P). The retrieved SWHs are compared with the European Centre for Medium-Range Weather Forecasts (ECMWF) reanalysis field at 0.125° grids. The root mean square error (RMSE) of SWH is 0.57m by using CSAR_WAVE2 is achieved, which is less than the analysis results achieved by using algorithm PFSM and Q-P. The statistical analysis also indicates that wind speed has little impact on bias with increasing wind speed. However, the retrieval tends to overestimate when SWH is smaller than 2.5m and

underestimate with increasing SWH. Moreover, the retrieval error grows with decreasing SWH at low state. This kind of behaviour gives a perspective of the improvement of SWH retrieval algorithm for GF-3 SAR acquired in wave mode.

1. Introduction

Gaofen-3 was launched by the China Academy of Space Technology (CAST) on August 2016 and is the first Chinese civilian satellite for scientific research, to carry synthetic aperture radar (SAR) at C-band as well as Canadian Radarsat-2 (R-2) and European Sentinel-1 (S-1). The National Ocean Satellite Application Center (NSOAS) is responsible for marine applications of GF-3 SAR. Through cooperation projects with NSOAS, some researchers have made a preliminary analysis of wind (Wang et al. 2017; Ren et al. 2017) and wave (Shao et al. 2017) retrieval from GF-3 SAR acquired in imaging mode, e.g., standard stripmap (SS) and quad-polarization mode (QPS-I/II) (vertical-vertical (VV); vertical-horizontal (VH); horizontal-horizontal (HH) and horizontal-vertical (HV)). In addition, the feasibility of retrieving sea surface wind speeds from VH-polarization GF-3 SAR acquired in global observation (GLO) and wide scanSAR (WSC) mode data with a large spatial coverage of more than 400km was recently reported in Shao et. al (2018), concluding that GF-3 SAR is a promising tool for the monitoring of strong winds under typhoon conditions.

Algorithms for wave retrieval have been well studied over previous decades (Chapron et al. 2001; Díaz-Méndez et al. 2010; Zhang et al. 2015). The algorithms used can be divided into three categories. The first two kinds are the theoretical-based algorithms exploited for co-polarization (VV or HH) and quad-polarization, both of which are based on the wave mapping mechanism on SAR. The SAR mapping mechanism includes tilt modulation (Lyzenga 1986), hydrodynamic modulation (Feindt et al. 1986) and velocity bunching (Alpers et al. 1981; Alpers and Bruning 1986). The other is an empirical algorithm, which allows direct retrieval of wave parameters from co-polarization SAR without calculating the modulation transfer function (MTF) of each SAR mapping modulation.

The first category includes the Max-Planck Institute Algorithm (MPI) (Hasselmann and Hasselmann 1991), the semi parametric retrieval algorithm (SPRA) (Mastenbroek and Valk 2000), the parameterized first-guess spectrum method (PFSM) (Sun and Guan 2006;) and the partition rescaling and shift algorithm (PARSA) (Schulz-Stellenfleth et al. 2005; Li et al. 2010), which are independent of radar frequency and polarization. These algorithms take a ‘first-guess’ wave spectrum in the inversion schemes, because the velocity bunching is a non-linear modulation causing signal loss in the azimuth direction. The MPI and PARSA algorithms use the simulations from a numeric wave model, which takes a considerable amount of time for model running in the operational application. The SPRA algorithm employs a wave spectrum produced by using a parameterized empirical function in the scheme, indicating it can be more conveniently applied than the MPI and PARSA algorithms. Subsequently, the PFSM algorithm was developed in order to overcome the model-induced error in the SPRA scheme system, which is included in the swell SAR spectrum. The improvement to the PFSM algorithm is that a prior SAR spectrum is divided into two portions, including wind-sea and linear-mapping swell. Through searching for the most suitable parameters, a best fit ‘first-guess’ spectrum is produced by a parametric wave model, which is similar to SPRA, and then an MPI scheme is employed for retrieving the wind-sea spectrum. The swell spectrum is obtained by directly inverting the linear-mapping SAR spectrum. Finally, the wave spectrum is composited of wind-sea and swell spectrum and then significant wave height (SWH) is calculated by integrating the SAR-derived wave spectrum. In our previous study, it was found that the PFSM algorithm worked for C-band (Lin et al. 2017) and X-band SAR (Shao et al. 2015) with an approximate 0.6m root mean square error (RMSE) of SWH.

The algorithm for quad-polarization (Q-P), which is the second category (Schuler et al. 2004; He et al. 2006; Zhang et al. 2010), is aimed at wave retrieval from SAR images such as the Q-P data acquired by R-2 and polarimetric SAR (POLSAR). These theoretical-based algorithms are exploited based on the wave slope estimation from SAR images in the co-polarization and HV-polarization channels. SWH is calculated by using the SAR-derived wave slope spectrum. Because GF-3 SAR wave mode data is available in quad-polarization, SWH can be measured by using the Q-P algorithm.

The empirical model is commonly used for marine applications of co-polarization SAR, and is classified as the third category. The CWAVE family was originally exploited by SAR oceanographyers at the German Aerospace Center (DLR), e.g., CWAVE_ERS (Schulz-Stellenfleth et al. 2007) for ERS-1/2 SAR and CWAVE_ENV (Li et al. 2011) for ENVISAT-ASAR, and can be applied for wave retrieval from SAR wave mode data at C-band without calculating the complex MTF of each SAR mapping modulation. The coefficients of the CWAVE model need to be refitted for a different SAR, such as the CWAVE_S1 for the European S-1 SAR (Stopa and Mouche, 2017). In addition, several recent studies have developed algorithms to retrieve SWH through the cutoff wavelength at C-band for R-2 (Ren et al. 2015), S-1 SAR (Shao et al. 2016; Grieco et al. 2016; Stopa and Mouche, 2017). In our recent study, an empirical algorithm is exploited for GF-3 SAR in co-polarization, named CSAR_WAVE2 (Sheng et al. 2018). CSAR_WAVE2 employs the basic formulation of the CWAVE model, in which the coefficients are tuned through 1523 GF-3 SAR QPS-I/II mode images with collocated European Centre for Medium-Range Weather Forecasts (ECMWF) reanalysis SWH data at 0.125° grids.

GF-3 SAR provides available data in wave mode for oceanic wave monitoring if request, similar to S-1 SAR, which has a about spatial coverage of around 5km×5km with a pixel size of 5m for azimuth direction and 4~6m for range direction. GF-3 SAR wave mode operates in quad-polarization with alternate incidence angle ranges from 20° to 50°, leading to adaptability of ocean observation, although small spatial coverage brings the limitation in the perspective of an operational ocean waves retrieval to some extent. In particular, the product derived from the SAR wave mode data is dedicated to oceanography research, particularly for global wave analysis (Li 2016). Therefore, for operational application, it is essential to establish the accuracy of the wave retrieval data for GF-3 SAR wave mode.

In this study, SWH is retrieved from quad-polarization GF-3 SAR wave mode data by using three algorithms, including PFSM, CSAR_WAVE2 and Q-P. Then assessment is presented as retrieval results are compared with the ECMWF reanalysis field at 0.125° grids. Our work shows the comparison of wave monitoring from the Chinese quad-polarization GF-3 SAR wave mode data with the European Centre for Medium-Range Weather Forecasts (ECMWF) reanalysis data and further recommend the algorithm for the operational wave retrieval. Moreover, the accuracy of retrieval SWH under various winds and sea states conditions is also studied in order to figure out the limitation and future improvement of wave retrieval algorithm for GF-3 SAR wave mode.

The remaining part of this paper is organized as follows: the datasets are briefly described in Section 2. Section 3 introduces the methodology of the theoretical-based and empirical wave retrieval algorithms used in this study. Then the validation of retrieval results is presented in Section 4. Section 5 shows the discussion and we give the summary in Section 6.

2. Brief description of data

The type of GF-3 SAR wave mode data is default processed as a Level-1A (L-1A) production, and was collected during the period August 2016 to January 2018. We take the following equation for calibrating the quad-polarization GF-3 SAR wave mode data.

$$\sigma_0 = DN^2 \times \left(\frac{M}{32767}\right)^2 \text{-}N \qquad [\text{dB}] \tag{1}$$

where σ_0 is the normalized radar cross (NRCS) united in dB, DN is the SAR-measured image intensity, M and N are the calibration constants stored in the annotated file.

To investigate the performance of the wave algorithms for GF-3 SAR wave mode, we also compared SAR-derived SWH with a 0.125×0.125° grid from the ECMWF reanalysis SWH data in this study. The ECMWF provides global reanalysis atmospheric and marine data for investigators world-wide, at a fine spatial resolution (up to a 0.125° grid) and at an interval of 6-hours per day. To date, ECMWF reanalysis data has proved a valuable source for developing and validating algorithms for SAR (Hersbach et al. 2007; Hersbach et al. 2010; Li et al. 2011; Shao et al. 2017).

Other marine phenomena may exist in the images, e.g., ice, upwelling and eddy, causing inhomogeneous patterns in the SAR scene. Therefore, homogeneous GF-3 SAR images acquired in wave mode were chosen in about 50% of the total cases, where the ratios of image variance and squared image mean values were smaller than 1.05 (Li et al. 2011). As examples, a homogeneous case taken at 06:54 UTC on 10 April 2017 and an inhomogeneous case at 02:36 UTC on 6 February 2017 are shown in Figures 1 and 2, respectively.

[Figure 1]

[Figure 2]

The geographical locations of all collected images are shown in Figure 3, in which the incidence angle for each image is indicated by the colour used, and Figure 4 shows the histogram of the wind speed, incidence angle, and SWH in the data collection. The available GF-3 SAR wave mode data for this study is presented in Table 1,in which 10514 GF-3 SAR imageries are used in order to evaluate the accuracy of SAR-derived SWH by using the three existing wave retrieval algorithms. Noted that the spatial coverage of dataset collected in the two years mission is limitedly, because GF-3 SAR wave mode only operates in request. Moreover, most imageries were taken at middle to high incidence angle, e.g., only 497 and 87 imageries at the incidence angle ranged from 20° to 25° and from 25° to 30° in the available dataset respectively, because we did the major quality control at such condition, which is common for other GF-3 SAR imaging modes in the duration of on-orbit calibration. In fact, the cooperation with NSOAS is in progress, for which GF-3 SAR wave mode covers the global sea within one month, and a lager dataset is anticipated.

[Table 1]

[Figure 3]

[Figure 4]

3. Methodology of wave retrieval algorithm

In this section, the principles of the three existing wave retrieval algorithms for co-polarization and quad-polarization, of PFSM, CSAR_WAVE2, and Q-P, are introduced.

3.1 The PFSM algorithm

SAR-derived wind speed U_{10} has first to be obtained as the PFSM algorithm is applied for retrieving waves from SAR images. The Geophysical model function (GMF) C-SARMOD (Mouche and Chapron 2015) is used here, and has the general formulation:

$$\sigma_0=B_0\times(1+B_1\times\cos\varphi+B_2\times\cos2\varphi) \quad (1)$$

where σ_0 is the SAR-measured NRCS usually expressed as a linear combination of three terms, B_s are functions of sea surface wind speed U_{10} and radar incidence angle θ, and φ is wind direction relative to range direction. Because two unknown variables exist in the C-SARMOD model, wind directions from the ECMWF reanalysis field at a 0.125° grid are directly employed. It should be noted that C-SARMOD is directly applicable for VV- and HH-polarization without using an extra polarization ratio (PR) model.

The PFSM algorithm scheme mainly includes two steps:

(1) The SAR intensity spectrum is obtained using the Fast Fourier Transformation (FFT) method on the original SAR data. Eq. (2) is used to calculate the separation wave number k_s. Then the SAR spectrum is divided into two portions, of nonlinear-mapping wind-sea and linear-mapping swell state.

$$k_s=\left(\frac{2.87\times g\times V^2}{R^2\times U_{10}^4\times\cos^2\varphi\times\left(\sin^2\varphi\times\sin^2\theta+\cos^2\varphi\right)}\right)^{0.33} \quad (2)$$

in which, g is the gravity acceleration, V is the satellite flight velocity, R is the slant range, U_{10} is the SAR-derived wind speed, θ is the radar incidence angle and φ is the angle of wave propagation direction relative to radar look direction.

(2) Wind-sea and swell spectra are retrieved from the corresponding portion of a SAR image spectrum. In the process of wind-sea retrieval, a 'first-guess' spectrum is generated using the parametric Jonswap model (Hasselmann and Hasselmann 1985) after searching for the most suitable parameters of wind wave spectrum, e.g., dominant wave phase velocity and wave propagation direction. Then, the wind wave spectrum is retrieved by minimizing the cost function (Hasselmann and Hasselmann 1991). In the meantime, it is convenient to invert the linear-mapping portion of a SAR image spectrum into a swell spectrum. SWH H_s is calculated through integrating the composite one-dimensional wave spectrum S_k in terms of wave number k by using Eq. (3).

$$H_s=4\sqrt{\int S_k dk} \quad (3)$$

A standard deviation (STD) of 0.67m was found when comparing retrieval results from 50 S-1 SAR images in VV-polarization with ECMWF reanalysis grids wave data around the China Seas (Lin et al. 2017).

3.2 CSAR_WAVE2

Theoretically, sea state is related to azimuthal cutoff wavelength (Hasselmann and Hasselmann 1991; Grieco et al. 2016; Stopa et al. 2016). Therefore, we proposed a semi-empirical algorithm for SWH retrieval, denoted as CSAR_WAVE, which was tuned through VV-polarization S-1 SAR images and collocated measurements from NDBC buoys of NOAA (Shao et al. 2016). In our recent study, the RMSE of SWH was found to be 0.58m using CSAR_WAVE when comparing the retrieved SWH from a few GF-3 SAR images in co-polarization with NDBC buoy measurements of NOAA (Shao et al. 2017).

In order to improve the accuracy of wave retrieval for GF-3 SAR, non-linear higher-order corrections on sea state are implemented in a new empirical algorithm, denoted as CSAR_WAVE2. CSAR_WAVE2 takes the basic formulation of the CWAVE family model, which assumes that sea state SWH can be connected by a set of imaging parameters with a coefficient vector (Schulz-Stellenfleth et al. 2007; Li et al. 2011; Stopa and Mouche, 2017). Schulz-Stellenfleth et al. (2007) found the RMSE of SWH to be 0.44m when using CWAVE with the second order model terms and this gives a better performance of 0.58m RMSE of the SWH when using the quadratic function for ERS-2 SAR wave mode.

The function of CSAR_WAVE2 is expressed as,

$$H_s=a_0+\sum_{i=1}^{n} a_i\times s_i+\sum_{i,j=1}^{n} a_{i,j}\times s_i\times s_j \tag{4}$$

in which s_i are the imaging parameters and vector $a_{i,j}$ ($i\leq j\leq n$) are the tuned coefficients. In practice, imaging parameters s_i in the CSAR_WAVE2 model include a vector (U_{10}, σ_0, $cvar$, λ_c/β, $sin\theta$, $cos2\varphi$, λ_{SAR}). U_{10} is the inverted wind speed, σ_0 is the SAR-measured NRCS, λ_c is the azimuthal cutoff wavelength estimated by fitting a one-dimensional SAR spectrum with a Gaussian fit function, θ is radar incidence angle φ peak wave direction relative to range direction ranged from 0° to 90°, β is the satellite range-to-velocity parameter, λ_{SAR} is the SAR length at peaks of the SAR spectrum and $cvar$ is the normalized SAR image stated as,

$$cvar=\mathrm{var}\left(\frac{I-\bar{I}}{\bar{I}}\right) \tag{5}$$

where, I is the pixel intensity of the SAR image and $\bar{I}$ is the mean of intensity.

It can be seen from our recent study (Sheng et al. 2018) that the RMSE of the SWH is about 0.52m for co-polarization GF-3 SAR imaging mode acquired in QPS-I/II when retrieval results are compared with the measurements from altimeter Jason-2. It was also found that CSAR_WAVE2 has a better performance of wave retrieval for GF-3 SAR than the analysis results achieved when using the other empirical algorithms proposed in Wang et al. (2012), Ren et al. (2015) and Grieco et al. (2016).

3.3 Algorithm Q-P

GF-3 wave mode is an available C-band SAR acquired in quad-polarization for wave monitoring over global seas. In recent years, efforts have been made to retrieve quantitative waves from quad-polarization SAR images (Schuler et al. 2004; He et al. 2006; Zhang et al. 2010).

The main principle of algorithm Q-P is that ocean waves sloping in the azimuth and range directions can be directly obtained using SAR data in the different polarization channels, e.g., HH-, VV- and HV-polarization. On the other hand, sea state is related to ocean wave slope. Taken together, SWH can be conveniently retrieved from a SAR-derived wave slope spectrum. The advantage of the Q-P algorithm is that wave parameters can be directly extracted from quad-polarization SAR images without estimating the complex hydrodynamic MTFs, similar to the empirical algorithms.

The Q-P algorithm procedure is illustrated as follows.

(1) Based on SAR images in the HH-, VV- and HV-polarization channel, the linearly polarized images σ_p are calculated using the following equation, in which the polarization orientation angle ψ is set as 45°.

$$\sigma_p=\frac{1}{4}(\sigma_{HH}+\sigma_{VV})\cdot[1+\cos^2(2\psi)]+\frac{1}{2}(\sigma_{HH}-\sigma_{VV})\cdot\begin{bmatrix}1+\cos(2\psi)+\\ \sigma_{HV}+\frac{1}{2}\times\Re[\ \sigma_{HHVV}]\times\sin^2(2\psi)\end{bmatrix} \quad (6)$$

in which σ_{VV}, σ_{HH}, and σ_{HV} represent the NRCS in the corresponding channel, σ_{HHVV} is correlated between HH- and VV- polarization and $\Re[\ ]$ represents the real parts of the indicated quantities.

(2) The wave slope spectrum ξ in range $\partial\xi/\partial x$ and azimuth direction $\partial\xi/\partial y$ is estimated using Eqs. (7a) and (7b),

$$\frac{\Delta\sigma_{VV}}{\overline{\sigma_{VV}}}-\frac{\Delta\sigma_{HH}}{\overline{\sigma_{HH}}}=-\frac{8\times\tan\theta}{1+\tan^2\theta}\times\frac{\partial\xi}{\partial x} \quad (7a)$$

$$\frac{\Delta\sigma_p}{\overline{\sigma_p}}-\frac{\Delta\sigma_{VV}}{\overline{\sigma_{VV}}}=A\times\frac{\partial\xi}{\partial x}+B\times\frac{\partial\xi}{\partial y} \quad (7b)$$

in which the coefficients A and B are referred to in Eq. 80 proposed in He et al. (2006).

(3) The root mean square slopes S_{rms} through the $\partial\xi/\partial x$ and $\partial\xi/\partial y$, together with the dominant wave propagation direction ϕ are calculated using the following equation,

$$S_{rms}=\sqrt{\left(\left\langle\frac{\partial\xi}{\partial x}\times\sin\phi\right\rangle\right)^{2}+\left(\left\langle\frac{\partial\xi}{\partial y}\times\cos\phi\right\rangle\right)^{2}} \tag{8}$$

(4) SWH H_s is calculated with Eq. (9),

$$H_s=2\sqrt{2}\times S_{rms} \tag{9}$$

4. Validations

In this section, we first present a comparison of the SAR-derived wind speed with ECMWF reanalysis data at 0.125° grids, as wind speed is directly related to sea state and is used in the wave retrieval algorithms. Then the retrieved SWHs are validated against the ECMWF reanalysis data by using the existing algorithms PFSM, CSAR_WAVE2 and Q-P.

4.1 Comparison of SAR-derived wind speed

The non-Bragg contribution on radar backscattering at VV-polarization is smaller than that at HH-polarization (Phillips et al. 2001; Kudryavtsev et al. 2003), which indicates that the wind and wave retrieval algorithms perform better at VV-polarization. Therefore, a comparison of retrieved wind speeds from GF-3 SAR images acquired in wave mode at VV-polarization is presented here.

As shown in Eq. (1), there are two unknown variables in the C-SARMOD. In this study, wind directions are obtained through ECMWF reanalysis data using the bilinear interpolation at temporal and spatial scales. Then wind speed can be retrieved from GF-3 SAR images acquired in wave mode. Figure 5 shows SAR-derived wind speeds using C-SARMOD versus wind speeds from ECMWF reanalysis data for 0.25m/s of wind speed bins between 0 and 15m/s. The RMSE of wind speed was found to be about 1.8m/s, which is close to the 1.6m/s and 1.4m/s RMSEs of wind speed against a few NDBC buoys of NOAA when C-SARMOD was applied for VV-polarization S-1 SAR (Lin et al. 2017) and GF-3 SAR (Shao et al. 2017) acquired in imaging mode. The worse performance here was probably caused by the use of different sources for validation. However, this still illustrates that SAR-derived wind speeds are reliable in the process of wave retrieval. It should be noted that the retrieved winds are smaller than 20m/s and do not have the backscattering signal problem encountered in the application of traditional GMF algorithms for wind retrieval at higher winds (Hwang et al. 2015).

[Figure 5]

4.2 Comparison of SAR-derived SWH

We first present the retrieval results of a sub-scene extracted from the images taken on 10 April 2017 at 06:54 UTC when using the existing three algorithms. In this case, the SWH from the ECMWF reanalysis data is 1.85m.

A quick-look image of the sub-scene covering the ECMWF locations at the 0.125°grid points is shown in Figure 6a as an example of retrieval results and the corresponding two-dimensional SAR spectrum is shown in Figure 6b. The SAR-derived SWH is 1.37m when using the PFSM algorithm through the retrieved one-dimensional wave spectrum exhibited in Figure 6c. The azimuthal cutoff wavelength λ_c is usually calculated by fitting a SAR spectrum with a Gaussian fit function $exp\{\pi(k_x/k_c)\}$, in which k_x is the azimuthal wavenumber and $k_c=2\pi/\lambda_c$ is the azimuthal cutoff wavenumber. Figure 6d shows the Gaussian fitted result of a sub-scene and the retrieved SWH is 2.37m using the CSAR_WAVE2 empirical algorithm. The SAR slope spectrum of the case is shown in Figure 7a and SAR-derived SWH is 1.45m using the Q-P algorithm through the retrieved one-dimensional wave slope spectrum, as exhibited in Figure 7b.

[Figure 6]

[Figure 7]

The collected sub-scenes from GF-3 SAR images were considered in order to evaluate the accuracy of SAR-derived SWH. The retrieved results were compared with ECMWF reanalysis data. In general, Figure 8 shows a 0.57m RMSE of SWH with a 0.22 scatter index (SI) using CSAR_WAVE2, which is less than a 0.63m RMSE with a 0.24 SI and a 0.71m RMSE with a 0.26 SI achieved using the PFSM algorithm and the Q-P algorithm respectively. It is not surprising that CSAR_WAVE has the best performance at low to moderate sea state, because CSAR_WAVE2 is directly tuned through GF-3 SAR data and the non-linearity among different imaging parameters has been included in the tune process of algorithm. A further comparison for a 1 m bin of SWH is also presented in Figure 8. It is found that RMSE of SWH is 0.47 m using PFSM algorithm and 0.43 m using CSAR_WAVE2 at SWH between 2m and 3m, which are less than that at other SWH ranges, however, Q-P algorithm has a worse performance (a 0.85 m RMSE) at such condition.

[Figure 8]

5. Discussions

We also analyze the applicability of the empirical algorithm CSAR_WAVE2 in various conditions. The bias (SAR-derived SWH minus SWH from ECMWF) versus the incidence angle and wind speed from ECMWF are shown in Figures 9a and 9b, respectively. A bin size of 2° for incidence angle and 1m/s for wind speed is used to group data pairs and the error bars represent the standard deviation of each bin. It is difficult to make state about the relation between the variation of bias and incidence angle. Interestingly, the variation of bias remains about 0.2m at wind speeds greater than 5m, indicating wind speed has little impact on bias with increasing wind speed.

[Figure 9]

The variation of bias as a function of SWH along with the ECMWF SWH for a bin size of 0.5m is presented in Figure 9c. It is roughly shown that the retrieved SWH over-estimates at SWH smaller than 2.5m and retrieved SWH has an underestimation at SWH greater than 2.5m. Nevertheless, it is clear to observe that the retrieval error grows with decreasing SWH at low state (SWH probably smaller than 2m). It is well known that cutoff wavelength in azimuth direction represents the velocity bunching mechanism, which is proportional to SWH (Hasselmann and Hasselmann 1991). Therefore, Bragg waves at sea surface with wavelength smaller than the cutoff wavelength in azimuth direction quantitively decrease under low sea state condition, due to cutoff wavelength in azimuth direction is relatively small at such condition. In other words, SAR backscattering signal is weak at low sea state. This is the probable explanation for the decreasing accuracy with decreasing SWH smaller than 2m, causing the limitation of CSAR_WAVE2. This issue needs to be resolved in the improvement of the wave retrieval algorithm for GF-3 SAR acquired in wave mode.

6. Summary

GF-3 SAR, operating in wave mode with alternate incidence angle, has the capability to monitor waves in global seas. At present, three algorithms, PFSM, CSAR_WAVE2 and Q-P, are consideratelly applied for wave retrieval from SAR images. As to release an operational product for global monitoring, it is necessary to select an optimal wave retrieval algorithm through evaluating the accuracy of SWH retrieval. Our work clarifies this issue through the comparison between the GF-3 image acquired in wave mode with the ECMWF model data, although taking advantage of limit dataset collected in the last two years mission.

A total of 10541 homogeneous cases from the collected images were selected, and these were matched up with ECMWF reanalysis data at 0.125°grids. GMF C-SARMOD was employed to retrieve winds for GF-3 SAR at VV-polarization, which was assumed to be prior information in the process of wave retrieval. The comparison shows a 1.8m/s RMSE of wind speed against the wind speed from the ECMWF reanalysis data, which is close to the accuracy of its application for S-1 SAR.

The 10514 images were processed using the three algorithms. The retrieved results were compared with SWH from ECMWF reanalysis wave data, and showed the RMSE of SWH to be 0.57m, 0.63m and 0.71m when using the PFSM, CSAR_WAVE2 and Q-P algorithms. However, we found that the SAR-derived SWH had a trend of saturation at SWH ranging up to 1.4m when using the Q-P algorithm, implying that retrieved SWH has an ambiguity under such conditions.

In summary, although our work shows that the CSAR_WAVE2 is recommended for use with GF-3 SAR data acquired in wave mode to date, we realize an improvement of the wave retrieval algorithm is still anticipated to ensure a better applicability for GF-3 SAR wave mode, especially the Chinese operational SAR satellite GF-3B and 3C plans to be launched at the end of 2019.

Acknowledgements

GF-3 SAR images are collected through an authorized account issued by NSOAS via http://dds.nsoas.org.cn. We also kindly appreciate ECMWF provides wind and wave data, which were openly downloaded via http://www.ecmwf.int. The research is partly supported by the National Key Research and Development Program of China under contract No. 2017YFA0604901, National Natural Science Foundation of China under contract No. 41806005, Public Welfare Technical Applied Research

Project of Zhejiang Province of China under contract No. LGF19D060003 and New-Shoot Talented Man Plan Project of Zhejiang Provence under contract No. 2018R411065.

6. References

Alpers, W., Ross, D. B. and Rufenach, C. L. 1981. “On the detectability of ocean surface waves by real and synthetic radar.” *Journal of Geophysical Research*, Vol. 86 (No. C7): pp. 6481–6498. doi: 10.1029/JC086iC07p06481.

Alpers, W. and Bruning, C. 1986. “On the relative importance of motion-related contributions to the SAR imaging mechanism of ocean surface waves.” *IEEE Transactions on Geosciences and Remote Sensing*, Vol. GE-24 (No. 6): pp. 873–885. doi: 10.1109/TGRS.1986.289702.

Chapron, B., Johnsen, H. and Garello, R. 2001. “Wave and wind retrieval from SAR images of the ocean.” *Annales Des Télécommunications*, Vol. 56 (No. 11): pp. 682–699. doi: 10.1007/BF02995562.

Feindt, F., Schroter, J. and Alpers, W. 1986. “Measurement of the ocean wave-radar modulation transfer function at 35GHz from a sea-based platform in the North Sea.” *Journal of Geophysical Research*, Vol. 91 (No. C8): pp. 9701–9708. doi: 10.1029/JC091iC08p09701.

Grieco, G., Lin, W., Migliaccio, M., Nirchio, F. and Portabella, M. 2016. “Dependency of the Sentinel-1 azimuth wavelength cut-off on significant wave height and wind speed.” *International Journal of Remote Sensing*, Vol. 37 (No. 21): pp. 9701–9708. pp. 5086–5104. doi: 10.1080/01431161.2016.1226525.

Hasselmann S. and Hasselmann K. 1985. “Computations and parametrizations of the nonlinear energy transfer in a gravity-wave spectrum. I: a new method for efficient computations of the exact nonlinear transfer integral.” *Journal of Physical Oceanography,* Vol. 15 (No. 1985): pp 1369–1377. doi: 10.1175/1520-0485(1985)015<1369:CAPOTN>2.0.CO;2.

Hasselmann, K. and Hasselmann, S. 1991. “On the nonlinear mapping of an ocean wave spectrum into a synthetic aperture radar image spectrum.” *Journal of Geophysical Research*, Vol. 96 (No. C6): pp.10713–10729. doi: 10.1029/91JC00302.

He, Y. J., Shen, H. and Perrie, W. 2006. “Remote sensing of ocean waves by polarimetric SAR.” *Journal of Atmospheric and Oceanic Technology*, Vol. 23 (No. 12): pp.1768–1773. doi: 10.1175/JTECH1948.1.

Hersbach, H., Stoffelen, A. and Haan, S. D. 2007. “An improved C-band scatterometer ocean geophysical model function: CMOD5.” *Journal of Geophysical Research*, Vol. 112 (No. C3): pp. C03006. doi: 10.1029/2006JC003743.

Hersbach, H. 2010. “Comparison of C-Band scatterometer CMOD5.N equivalent neutral winds with ECMWF.” *Journal of Atmospheric and Oceanic Technology*, Vol. 27 (No. 4): pp. 721–736. doi: 10.1175/2009JTECHO698.1.

Hwang, P. A. and Fois, F. 2015. “Surface roughness and breaking wave properties retrieved from polarimetric microwave radar backscattering.” *Journal of Geophysical Research*, Vol. 120 (No. 5): pp. 3640–3657. doi: 10.1002/2015JC010782.

Lyzenga, D. R. 1986. “Numerical simulation of synthetic aperture radar image spectra for ocean waves.” *IEEE Transactions on Geosciences and Remote Sensing*, Vol. GE-24 (No. 6): pp. 863–872. doi: 10.1109/TGRS.1986.289701.

Li, X. M., Konig, T., Schulz-Stellenfleth, J. and Lehner, S. 2010. “Validation and intercomparison of ocean wave spectra inversion schemes using ASAR wave mode data.” *International Journal of Remote Sensing*, Vol. 31 (No. 17): pp. 4969–4993. doi: 10.1080/01431161.2010.485222.

Díaz-Méndez, G. M., Lehner, S., Ocampo-Torres, F. J., Li, X. M. and Brusch, S. 2010. “Wind and wave observations off the south Pacific Coast of Mexico using TerraSAR-X imagery.” *International Journal of Remote Sensing*, Vol. 31 (No. 17): pp. 4933–4955. doi: 10.1080/01431161.2010.485217.

Li, X. M., Lehner, S. and Bruns, T. 2011. “Ocean wave integral parameter measurements using Envisat ASAR wave mode data.” *IEEE Transactions on Geosciences and Remote Sensing*, Vol. 49 (No. 1): pp. 155–174. doi: 10.1109/TGRS.2010.2052364.

Li, X. M. 2016. “A new insight from space into swell propagation and crossing in the global oceans.” *Geophysical Research Letters*, Vol. 43 (No. 10): pp. 5202–5209. doi: 10.1002/2016GL068702.

Lin, B., Shao, W. Z., Li, X. F., Li, H., Du, X. Q., Ji, Q. Y. and Cai L. N. 2017. “Development and validation of an ocean wave retrieval algorithm for

VV-polarization Sentinel-1 SAR data.” *Acta Oceanologica Sinica*, Vol. 36 (No. 7): pp. 95–101. doi: 10.1007/s13131-017-1089-9.

Mastenbroek, C. and Valk, C. F. de. 2000. “A semi-parametric algorithm to retrieve ocean wave spectra from synthetic aperture radar.” *Journal of Geophysical Research*, Vol. 105 (No. C2): pp. 3497–3516. doi: 10.1029/1999JC900282.

Mouche, A.A. and Chapron, B., 2015. “Global C-Band Envisat, RADARSAT-2 and Sentinel-1 SAR measurements in co-polarization and cross-polarization.” *Journal of Geophysical Research*, Vol. 120 (No. 11): pp. 7195–7207. doi: 10.1002/2015JC011149.

Kudryavtsev, V., Hauser, D., Caudal, G. and Chapron B. 2003. “A semiempirical model of the normalized radar cross section of the sea surface, 2. Radar modulation transfer function.” *Journal of Geophysical Research*, Vol. 108 (No. C3): pp. FET 3-1– FET 3-16. doi: 10.1029/2001JC001004.

Phillips, O. M., Posner, F. L. and Hansen, J. P. 2001. “High range resolution radar measurements of the speed distribution of breaking events in wind-generated ocean waves: surface impulse and wave energy dissipation rates.” *Journal Physical Oceanography*, Vol. 31(No. 2): 450–460. doi: 10.1175/1520-0485(2001)031<0450:HRRRMO>2.0.CO;2.

Ren, L., Yang, J. S., Zheng, G. and Wang, J. 2015. “Significant wave height estimation using azimuth cutoff of C-band RADARSAT-2 single-polarization SAR images.” *Acta Oceanologica Sinica*, Vol. 34 (No. 12): pp. 1–9. doi: 10.1007/s13131-015-0769-6.

Ren, L., Yang J. S., Mouche, A. A., Wang, H., Wang, J. and Zheng, G. 2017. “Preliminary analysis of Chinese GF-3 SAR quad-polarization measurements to extract winds in each polarization.” *Remote Sensing*, Vol. 9 (No. 12): pp: 1215. doi: 10.3390/rs9121215.

Schuler, D. L., Lee, J. S., Kasilingam, D. and Pottier, E. 2004. “Measurement of ocean surface slopes and wave spectra using polarimetric SAR image data.” *Remote Sensing of Environment*, Vol. 91 (No. 2): pp: 198–211. doi: 10.3390/rs9121215.

Schulz-Stellenfleth, J., Lehner, S. and Hoja, D. 2005. “A parametric scheme for the retrieval of two-dimensional ocean wave spectra from synthetic aperture radar look cross spectra.” *Journal of Geophysical Research*, Vol. 101 (No. C5): pp. 297–314. doi: 10.1016/j.rse.2004.03.008.

Schulz-Stellenfleth, J., Konig, T. and Lehner, S. 2007. “An empirical approach for the retrieval of integral ocean wave parameters from synthetic aperture radar data.” *Journal of Geophysical Research*, Vol. 42 (No. 34): pp. 10182−10190. doi: 10.1029/2006JC003970.

Shao W. Z., Li, X. F. and Sun J. 2015. “Ocean wave parameters retrieval from TerraSAR-X images validated against buoy measurements and model results.” *Remote Sensing*, Vol. 7 (No. 10): pp. 12815. doi: 10.3390/rs71012815.

Shao, W. Z., Zhang, Z., Li X. F. and Li, H. 2016. “Ocean wave parameters retrieval from Sentinel-1 SAR imagery.” *Remote Sensing*, Vol. 8 (No. 9): pp. 707. doi: 10.3390/rs8090707.

Stopa J. E., Ardhuin, F., Chapron, B. and Collard, F. 2016. “Estimating wave orbital velocity through the azimuth cutoff from space-borne satellites.” *Journal of Geophysical Research Oceans*, Vol. 120 (No. 11): pp 7616–7634. doi: 10.1002/2015JC011275.

Shao, W. Z., Shen, Y. X. and Sun, J. 2017. “Preliminary assessment of wind and wave retrieval from Chinese Gaofen-3 SAR imagery.” *Sensors*, Vol. 17 (No. 8): pp. 1705. doi: 10.3390/s17081705.

Stopa, J. E. and Mouche, A. 2017. “Significant wave heights from Sentinel-1 SAR: validation and applications.” *Journal of Geophysical Research Oceans*, Vol. 122 (No. 3): pp. 1827−1848. doi: 10.1002/2016JC012364.

Shao, W. Z., Yuan, X. Z., Sheng, Y. X., Sun, J., Zhou, W. and Zhang, Q. J. 2018. “Development of wind speed retrieval from cross-polarization Chinese Gaofen-3 synthetic aperture radar in typhoons.” *Sensors*, Vol. 18 (No. 2): pp. 412. doi: 10.3390/s18020412.

Wang, H., Yang, J. S., Mouche, A. A., Shao, W. Z., Zhu, J. H., Ren, L. and Xie, C. H. 2017. “GF-3 SAR ocean wind retrieval: The first view and preliminary assessment.” *Remote Sensing*, Vol. 9 (No. 7): pp. 694−706. doi: 10.3390/rs9070694.

Sheng Y. X., Shao, W. Z., Zhu, S., Sun, J., Yuan, X. Z., Li, S. Q., Shi, J. and Zuo J. C. 2018. “Validation of significant wave height retrieval from co-polarization Chinese Gaofen-3 SAR imagery by using an improved algorithm.” *Acta Oceanologica Sinica*, Vol. 37 (No. 6): pp. 1−10. doi: 10.1007/s1313.

Zhang, B., Perrie, W. and He, Y. J. 2010. “Validation of RADARSAT-2 fully polarimetric SAR measurements of ocean surface waves.” *Journal of*

Geophysical Research, Vol. 116 (No. C6): pp. 302–315. doi: 10.1029/2009JC005887.

Zhang, B., Li, X. F., Perrie, W., and He, Y. J. 2015. “Synergistic measurements of ocean winds and waves from SAR.” *Journal of Geophysical Research Oceans*, Vol. 120 (No. 9): pp. 6164–6184. doi: 10.1002/2015JC011052.

Table 1 Available Gaofen-3 (GF-3) SAR wave mode data in this study

ID	Incidence angle			Numbers of GF-3 imageries in wave mode
	Range	Mean	Standard deviation	Available numbers
WV01	20°-25°	21.93°	0.90°	497
WV02	25°-30°	28.22°	0.26°	87
WV03	30°-35°	31.30°	1.37°	1919
WV04	35°-40°	36.76°	1.20°	4605
WV05	40°-45°	42.35°	1.64°	2191
WV06	45°-50°	47.08°	1.45°	1215

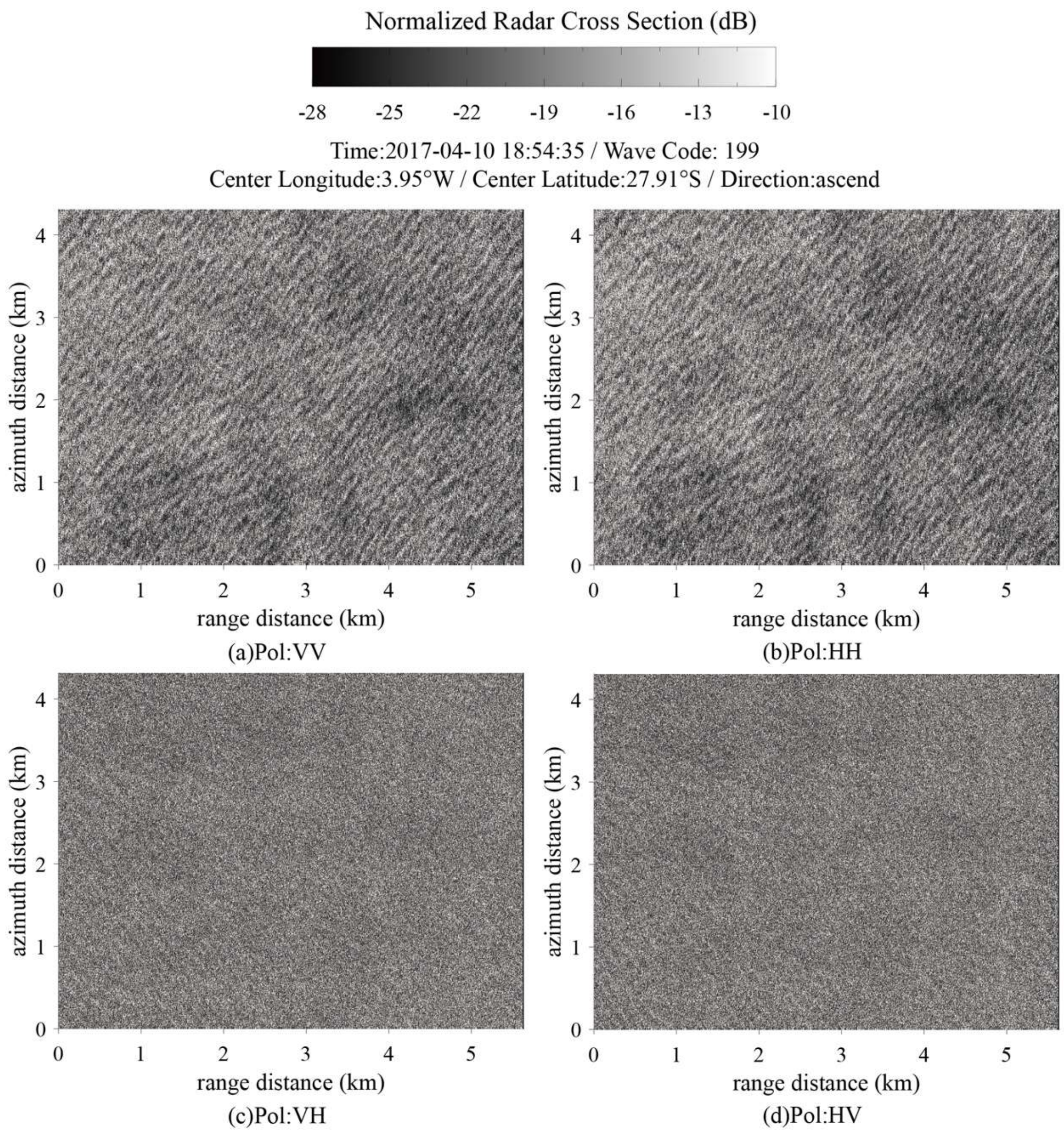

Fig.1 An example of GF-3 SAR wave mode data with homogeneous wave streaks taken at 06:46 UTC on 8 March 2017 after calibration. (a) VV-polarization. (b) HH-polarization. (c) VH-polarization. (d) HV-polarization

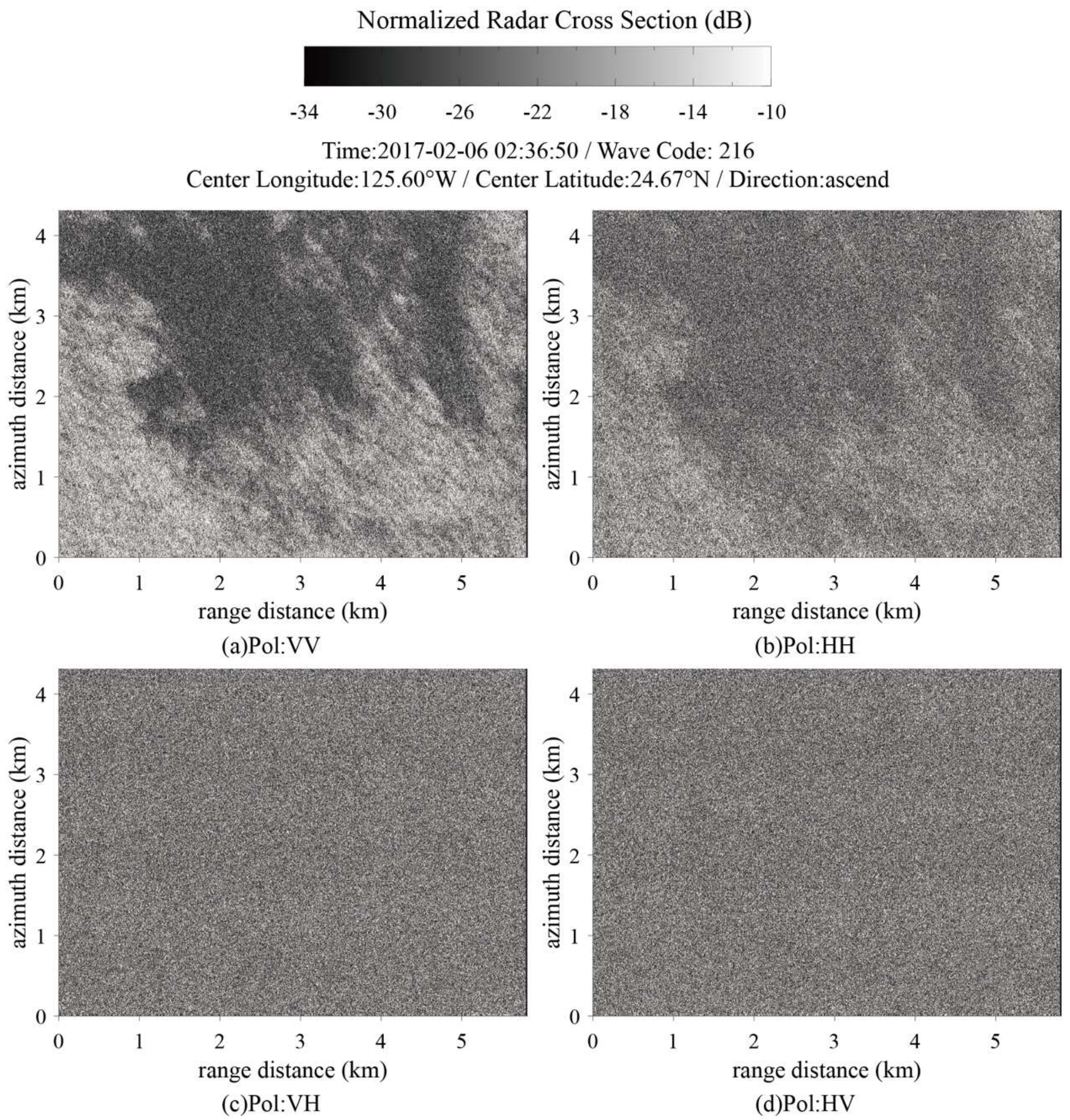

Fig.2 An example of GF-3 SAR wave mode data with inhomogeneous wave streaks taken at 02:36 UTC on 6 February 2017 after calibration. (a) VV-polarization. (b) HH-polarization. (c) VH-polarization. (d) HV-polarization

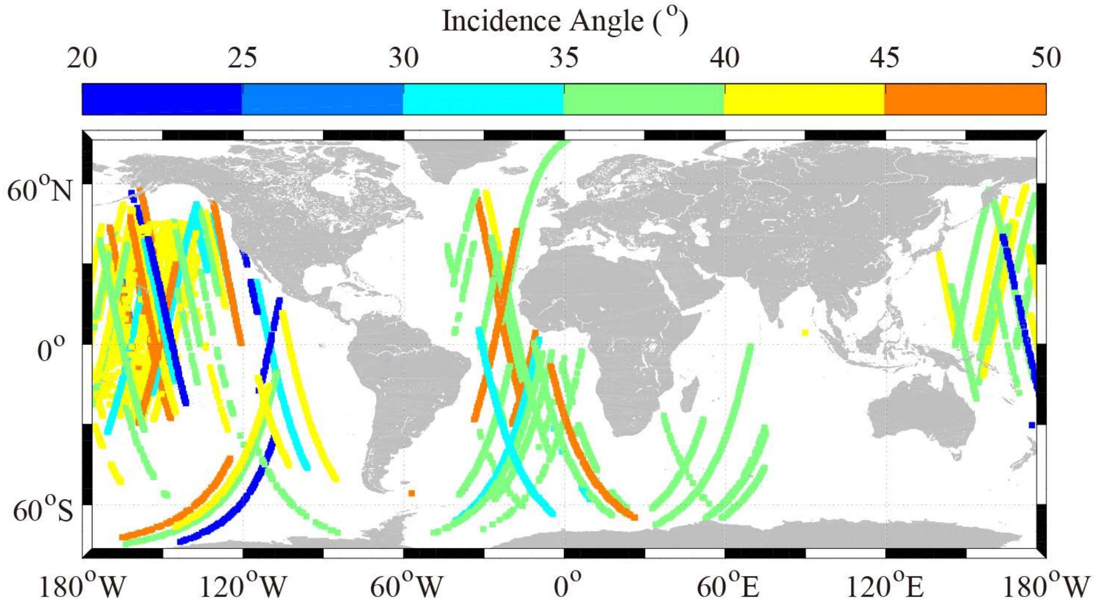

Fig.3 The geographical locations of all available GF-3 SAR imageries acquired in wave mode, in which that colors show the approximate incidence angle of each imagery.

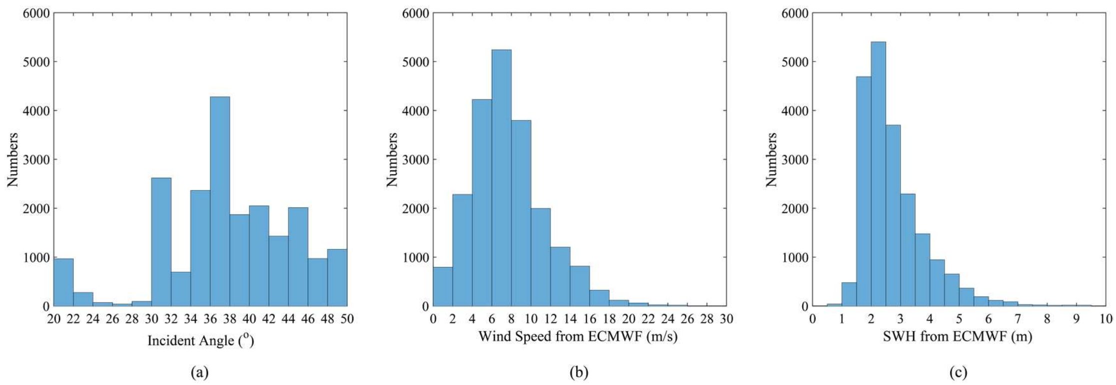

Fig.4 (a) The histogram of incidence angle for the collected images. (b) The histogram of wind speed for the collected images. (c) The histogram of significant wave height for the collected images.

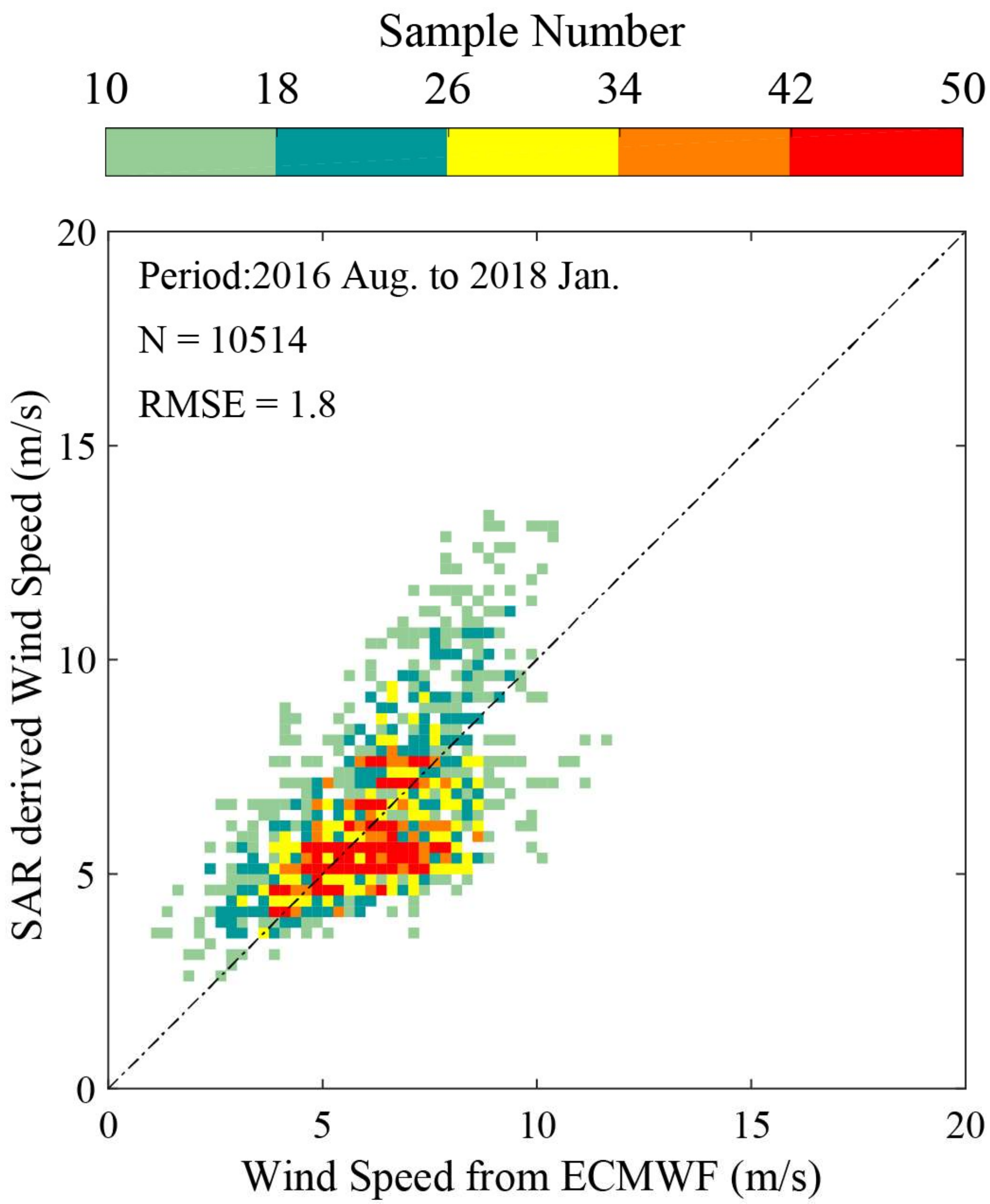

Fig.5 SAR-derived wind speeds using the C-SARMOD wind retrieval algorithm versus wind speeds from ECMWF reanalysis data for 0.25m/s of wind speed bins between 0 and 15m/s.

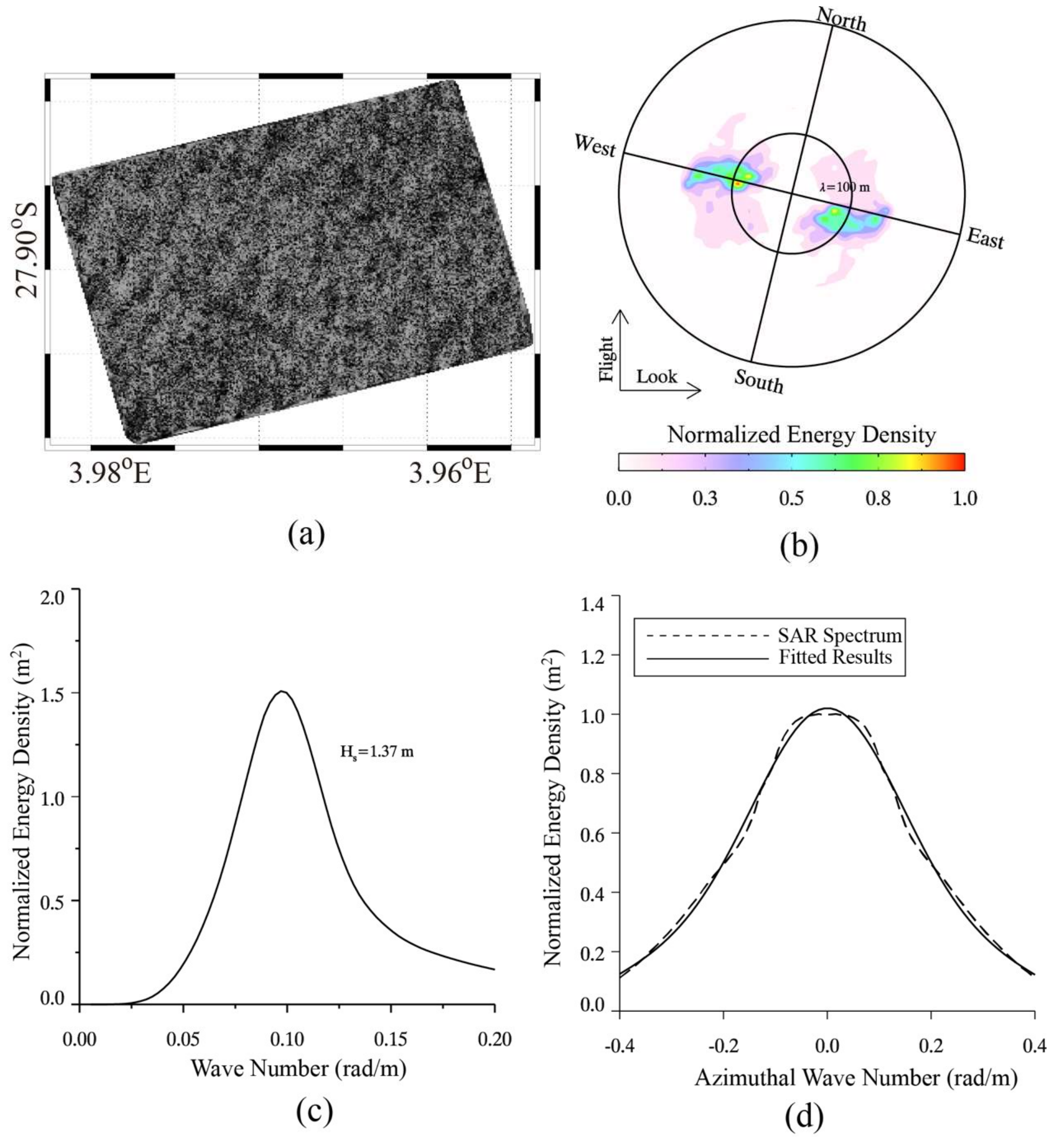

Fig.6 (a) The sub-scene extracted from the case in VV-polarization, which was taken on 10 April 2017 at 06:54 UTC. (b) The two-dimensional SAR spectra of sub-scene in polar coordinate. (c) The SAR-derived one-dimensional wave of sub-scene. (d) The Gaussian fit result of sub-scene.

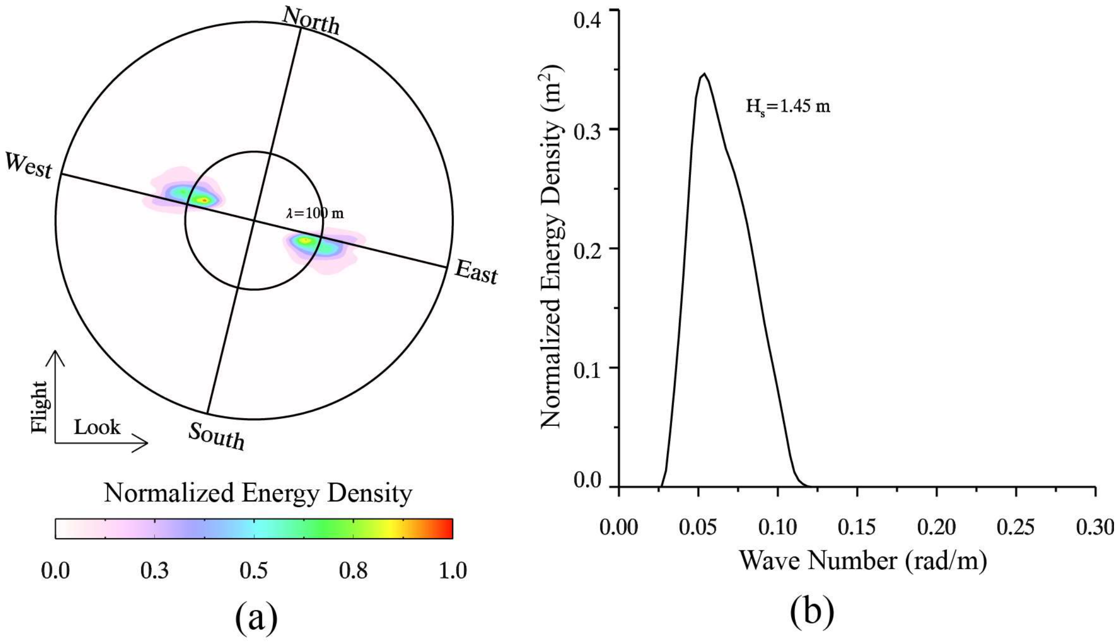

Fig.7 (a) The two-dimensional SAR slope spectrum of sub-scene in polar coordinate which was taken on 10 April 2017 at 06:54 UTC. (b) The SAR-derived one-dimensional wave slope spectrum of sub-scene.

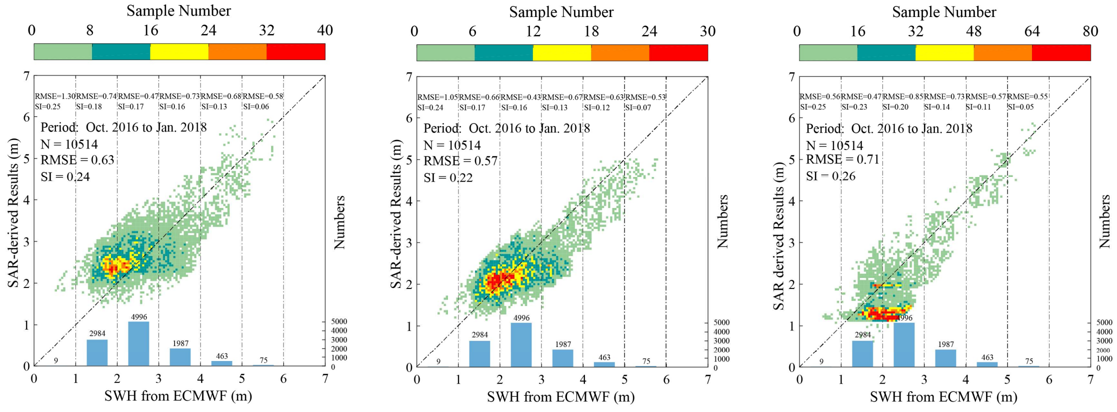

(a) (b) (c)

Fig.8 SAR-derived results versus SWH from ECMWF reanalysis data for 0.05m of SWH bins between 0 and 6m when using the three existing algorithms. (a) Algorithm PFSM. (b) C Algorithm SAR_WAVE2. (c) Algorithm Q-P.

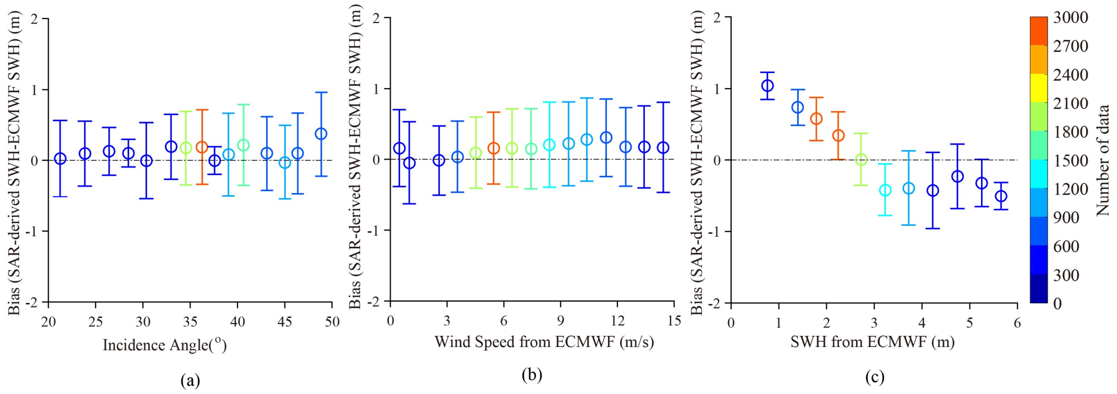

Fig.9 Variation of bias between SAR-derived SWH by using CSAR_WAVE2 and other parameters. (a) Incidence Angle. (b) ECMWF Wind Speed. (c) ECMWF SWH.